

# Broadband telecom transparency of semiconductor-coated metal nanowires: more transparent than glass

R. Paniagua-Domínguez,<sup>1</sup> D. R. Abujetas,<sup>1</sup> L. S. Froufe-Pérez,<sup>1</sup> J. J. Sáenz,<sup>2</sup> and J. A. Sánchez-Gil<sup>1</sup>

<sup>1</sup>*Instituto de Estructura de la Materia, Consejo Superior de Investigaciones Científicas, Serrano 121, 28006 Madrid, Spain*

<sup>2</sup>*Condensed Matter Physics Dept. and Centro de Investigación en Física de la Materia Condensada (IFIMAC), Universidad Autónoma de Madrid, Fco. Tomás y Valiente 7, 28049-Madrid, Spain*

Metallic nanowires (NW) coated with a high permittivity dielectric are proposed as means to strongly reduce the light scattering of the conducting NW, rendering them transparent at infrared wavelengths of interest in telecommunications. Based on a simple, universal law derived from electrostatics arguments, we find appropriate parameters to reduce the scattering efficiency of hybrid metal-dielectric NW by up to three orders of magnitude as compared with the scattering efficiency of the homogeneous metallic NW. We show that metal@dielectric structures are much more robust against fabrication imperfections than analogous dielectric@metal ones. The bandwidth of the transparent region entirely covers the near IR telecommunications range. Although this effect is optimum at normal incidence and for a given polarization, rigorous theoretical and numerical calculations reveal that transparency is robust against changes in polarization and angle of incidence, and also holds for relatively dense periodic or random arrangements. A wealth of applications based on metal-NWs may benefit from such invisibility.

## I. INTRODUCTION

In recent years, plasmonic cloaking has received considerable attention as a mechanism to dramatically reduce the electromagnetic scattering cross section of an object [1–3]. State of the art technology allows for the fabrication of building blocks for optical materials which shape, size and composition can be chosen among a large variety, giving rise to nanostructured engineered materials with prescribed optical properties. The optical response of the material in a certain frequency range is often based on the appearance of resonances in the building blocks; hence, the delicate interplay among all the parameters controlling the systems response must be considered. Even relatively simple systems, such as high refractive index homogeneous dielectric spheres, show interesting light scattering properties arising from the excitation of single Mie resonances or superpositions of different ones [4]. Interestingly, only in the last years some of those well known properties have been put forward and measured experimentally [5–8].

Going one step further, more degrees of freedom can be obtained if core-shell structures are considered [9]. The interaction among the modes supported by the different layers together with size control and materials properties, even presenting magnetism [10], lead to a certain tunability of Mie resonances that can result, for instance, in the superposition of electric and magnetic dipole resonance leading to a certain directivity control in the light scattering by a submicron particle [11]. Suitable configurations of such particles have been proposed for high directivity, low absorption optical antennas [12]. Also, tuning of plasmon resonances in core-shell hybrid metal-dielectric nanospheres, leads to a large control on the absorption spectrum of nanoparticles [13]. Systems presenting extremely low scattering cross-sections were proposed decades ago [14] for absorptionless dielectric materials and, more recently, similar geometries were used as cloaks for metallic spherical structures [15–17].

Considering available technologies, the use of cylindrical structures is better suited for many optics and optoelectronics [18] applications ranging from nanoantenna emission [19] to invisible fibers [20], cloaking devices [21–25], superscattering structures [24], or low loss negative index materials [26]. The most widespread used materials are semiconductors and metals [27]. This kind of structures have been demonstrated to be suitable building blocks for multifunctional materials. ZnO/Ag nanowire composites [28] have been recently presented as good candidates to fabricate high electrical conductivity and good optical transparency electrodes with a potential impact in several industrial applications [29]. Also growth-controlled semiconductor NWs with different sizes and geometries have been proposed as means to control light absorption in photovoltaic applications [30].

Different two and three dimensional plasmonic cloaking structures have been proposed in the literature and experimentally demonstrated all the way from radio frequency to the optical ranges. Metal coated dielectric cylinders [3] have been recently used as a suitable implementation of a cloaked sensor [31]. This cloaking mechanism can present several advantages over other approaches: it can be achieved with homogeneous and isotropic materials and the underlying physical mechanism does not depend on resonances, but on the cancellation of the average polarization density in the object. Hence, fabrication of actual structures for the infrared and optical ranges should be eased by the availability of materials and robustness against manufacturing defects.

Although comprehensive descriptions of the conditions leading to extremely small light scattering efficiency in hybrid metal-dielectric NWs [21] or spheres [16, 17] is available in the literature, several relevant aspects have been

overlooked so far. In particular, using dielectric coated metallic NWs might seem similar, if not equivalent, to its inverse structure, namely, metal coated dielectric NWs. Nevertheless, we shall show that this is not the case and that the former structure is much more robust regarding geometrical variations. On the other hand, a deeper analysis of the near field multiple scattering among transparent structures is still lacking in the literature. It is the purpose of this manuscript to perform such an analysis.

In this work, we analyze in detail the conditions required to obtain small scattering efficiency in a core-shell cylinder for any metal or dielectric combination throughout remarkably broad bands in the IR spectral region relevant to telecommunications [32]. By the use of a simple model based on the quasi-static approximation with radiative corrections to the polarizability of a core-shell cylinder [33], we obtain general properties required to achieve transparency in realistic structures [21]. We also check our predictions against a more accurate model based on Mie theory for coated cylinders [34, 35]. We find that, under rather general conditions, metal nanowires with high refractive index coatings can show a transparency region which is more robust against fabrication defects (size polydispersity) than metal coated fibers. Also, it is shown that it is possible to obtain up to three orders of magnitude lower scattering efficiency, compared with raw metal cylinders, in a band as wide as 20% of the central frequency, and with realistic materials (Si coated Ag wires) in the infrared. The transparency condition is also quite robust regarding the angle of incidence and polarization of the incoming signal. It is shown that the near field scattering is extremely weak in the transparency region. Hence, the coupling through evanescent modes among cylinders is essentially negligible. As a consequence, a high density assembly of appropriately designed NWs present an extremely low scattering efficiency. For the sake of comparison, we show that a properly designed coating for a metal NW with a given diameter, can present smaller scattering efficiency than a glass slab of equivalent thickness.

## II. TRANSPARENCY CONDITIONS

For normal incidence and transverse magnetic (TM) polarized plane waves, the electric field in the electrostatic approximation is constant and parallel to the cylinder axis. The quasi-static polarizability in this case is

$$\alpha_0^{(TM)} = A [(\epsilon_c - \epsilon_h) R^2 + (\epsilon_s - \epsilon_h) (1 - R^2)] \quad (1)$$

where  $A = \pi R_s^2$  is the total cross section of the cylinder and  $R \equiv R_c/R_s$  is the ratio of the core to shell radii. Throughout this paper, sub-index  $h$  refers to the host medium,  $s$  to the shell medium, and  $c$  to the core medium; to depict the structures, we shall use core-material@shell-material notation (for instance Ag@Si denotes a silver core NW coated with silicon). The quasi-static polarizability given by Eq. (1) can be interpreted as the cross-section averaged susceptibility. Interestingly, the quasi-static polarizability (1) is invariant if we exchange  $\epsilon_c$  with  $\epsilon_s$ , and  $R^2$  with  $(1 - R^2)$ . In fact, the quasi-static polarizability is proportional to the cross-section average of the polarizability density in the quasi-static approximation. Hence if the relative amount of metal and dielectric is kept constant, any spatial distribution of both components would lead to the same polarizability. This fact establishes a correspondence between metal@dielectric and dielectric@metal NWs.

A radiative correction to the quasi-static polarizability must be included in order to obtain a correct energy balance between scattering, absorption and extinction in the scattering process. The dynamic polarizability in the small particle approach is  $\alpha^{(TM)} = \alpha_0^{(TM)} / (1 - ik_h^2 \alpha_0^{(TM)} / 4)$  from which the scattering efficiency can be obtained as

$$Q_{scat}^{(TM)} = |\alpha^{(TM)}|^2 k_h^3 / (8\epsilon_h^2 R_s). \quad (2)$$

From Eq. (1), the scattering efficiency presents a minimum for a size ratio  $R = R_{tr}^{(TM)}$  such that

$$\left(R_{tr}^{(TM)}\right)^2 = \frac{\epsilon_h - \epsilon'_s}{\epsilon'_c - \epsilon'_s} \quad (3)$$

where primes in the above expression indicate the real part of the permittivity (the host material is assumed to be absorptionless). When this transparency condition is fulfilled, the averaged polarization density in the cross section of the cylinder vanishes.

Several cases can be discussed depending on the nature of the materials. For metal@dielectric cylinders, we consider  $\epsilon'_c < 0$  and  $\epsilon'_s > \epsilon_h > 0$ , leading to  $R_{tr}^{TM} < 1$ ; i.e. any metal core and dielectric shell with refractive index larger than the host medium presents an optimum size ratio  $R_{tr}^{TM}$  for transparency. In the inverse case, dielectric@metal, there is an optimum size ratio  $R_{tr}$  if the dielectric core presents a refractive index higher than the host medium. On the other hand, pure dielectric structures can also show transparency if  $\epsilon'_s > \epsilon_h > \epsilon'_c$  or  $\epsilon'_c > \epsilon_h > \epsilon'_s$ . Obviously, these

latter two conditions can not be fulfilled in vacuum. For purely metallic structures, there is no optimum ratio even in the absorptionless limit.

Analogously, we analyze also the TE polarization. In this case, considering the matching of the electric field at the boundaries, we obtain a quasi-static polarizability

$$\alpha_0^{(TE)} = 2A \frac{(\epsilon_s - \epsilon_h)(\epsilon_s + \epsilon_c) + (\epsilon_c - \epsilon_s)(\epsilon_h + \epsilon_s)R^2}{(\epsilon_s + \epsilon_h)(\epsilon_s + \epsilon_c) - (\epsilon_c - \epsilon_s)(\epsilon_h - \epsilon_s)R^2}. \quad (4)$$

The polarizability with radiative correction reads in this case,  $\alpha^{(TE)} = \alpha_0^{(TE)} / \left(1 - ik_h^2 \alpha_0^{(TE)} / 8\right)$ , and the scattering efficiency,

$$Q_{scat}^{(TE)} = \left| \alpha^{(TE)} \right|^2 k_h^3 / (16\epsilon_h^2 R_s). \quad (5)$$

The optimum size ratio  $R = R_{tr}^{(TE)}$  that minimizes the scattering is reached for vanishing quasi-static polarizability; in this case the optimum size is

$$\left( R_{tr}^{(TE)} \right)^2 = \frac{(\epsilon_h - \epsilon'_s)(\epsilon'_c + \epsilon'_s)}{(\epsilon_h + \epsilon'_s)(\epsilon'_c - \epsilon'_s)} = \left( R_{tr}^{(TM)} \right)^2 \frac{(\epsilon'_s + \epsilon'_c)}{(\epsilon'_s + \epsilon_h)}. \quad (6)$$

Both Eqs. (3) and (6) are in full agreement with the ones obtained in [21]. Contrary to the TM polarization case, Eq. (6) for TE polarization is more restrictive regarding materials. For metal@dielectric it is not always possible to obtain an optimum size ratio minimizing light scattering in TE polarization. If  $|\epsilon'_c| > \epsilon'_s$ , which is a typical case in the optical and infrared for many metals and available dielectrics, the ratio given by Eq. (6) is negative and hence the solution is unphysical.

On the other hand, it is clear from Eqs. (3) and (6) that it is not possible to minimize the scattering efficiency for a single core-shell structure at both TM and TE polarizations at the same wavelength. However, we will show later on that the TM transparency condition spectrally overlaps with a region of weak TE scattering efficiency, thus leading to highly polarization-independent transparency.

Nevertheless, the situation changes for dielectric@metal structures. An optimum size ratio  $R_{tr}^{(TE)}$  can be reached with realistic materials. In this case, we can also expect the appearance of a localized surface plasmon (LSP) resonance near the condition of minimum scattering efficiency. It can be shown that, in the limit  $\epsilon'_c \gg \epsilon_h$  (for instance, semiconductor core) and  $|\epsilon'_s|^2 \gg \epsilon'_c \epsilon_h$  (common with noble metals as shell material), the wavelength of the LSP resonance  $\lambda_{lsp}$  is shifted with respect to the chosen wavelength for transparency  $\lambda_{tr}$  by an amount  $(d\epsilon'_s/d\lambda)|_{\lambda=\lambda_{tr}} (\lambda_{lsp} - \lambda_{tr}) \simeq \epsilon_h/\epsilon_c$ . Hence, metal shells with large chromatic dispersion and high refractive index dielectric cores can lead to a spectrally sharp LSP-to-transparency transition. We postpone the study of its implications to a further work.

For dielectric@metal structures at fixed wavelength, there is also an optimum size ratio  $R = R_{lsp}^{(TE)}$  for which the LSP resonance matches the selected wavelength. Again considering the divergence of the quasi-static polarizability we obtain

$$\Delta R \equiv \frac{R_{tr}^{(TE)} - R_{lsp}^{(TE)}}{R_{tr}^{(TE)} + R_{lsp}^{(TE)}} = \left| \frac{\epsilon_h}{\epsilon'_s} \right| \quad (7)$$

For instance, at  $\lambda = 1550$  nm, a Si@Ag cylinder in vacuum presents a ratio  $\Delta R = 1/130 \simeq 7.7 \times 10^{-3}$ . Hence, relatively small deviations from the optimum size ratio would have a large impact in the scattering efficiency spectrum.

To illustrate the results of this section, we plot in Fig. 1 the scattering efficiency from Eqs. (2) and (5) of core-shell nano-cylinders considering TM and TE polarizations and unpolarized radiation for both metal@dielectric and dielectric@metal configurations [sketched in Fig. 1(a)]. We have chosen silicon as a suitable semiconductor in the infrared, and silver as the metallic component. In the spectral region of interest, we use  $\epsilon_{Si} = 12.25$ , whereas  $\epsilon_{Ag}$  is taken from [36].

In Fig. 1(b),  $Q_{scat}$  is shown as a function of the size ratio  $R = R_c/R_s$  at a working wavelength  $\lambda = 1550$  nm ( $\epsilon_{Ag} \simeq -130 + 3.3i$ ). As predicted by Eq. (3),  $Q_{scat}$  for TM polarization (dashed lines) presents a sharp minimum when the cross-sectional average of the electric polarization density vanishes. In the case under study, this condition is fulfilled when the Ag to Si volume ratio is  $V_{Ag}/V_{Si} = (\epsilon'_{Si} - 1) / (\epsilon'_{Ag} - 1) \simeq 0.086$ , which corresponds to  $R_{tr}^{TM} \simeq 0.28$  for a Ag@Si NW, and  $R_{tr}^{TM} \simeq 0.96$  for a Si@Ag NW. Both values of the optimum size ratio for transparency are represented by vertical lines in Fig. 1(b).

For TE polarization, as predicted by Eq. (6), there is no optimum size ratio minimizing  $Q_{scat}$  at the working wavelength for Ag@Si NWs, but it shows a weak monotonic increase with  $R$ . On the contrary, for Si@Ag NWs

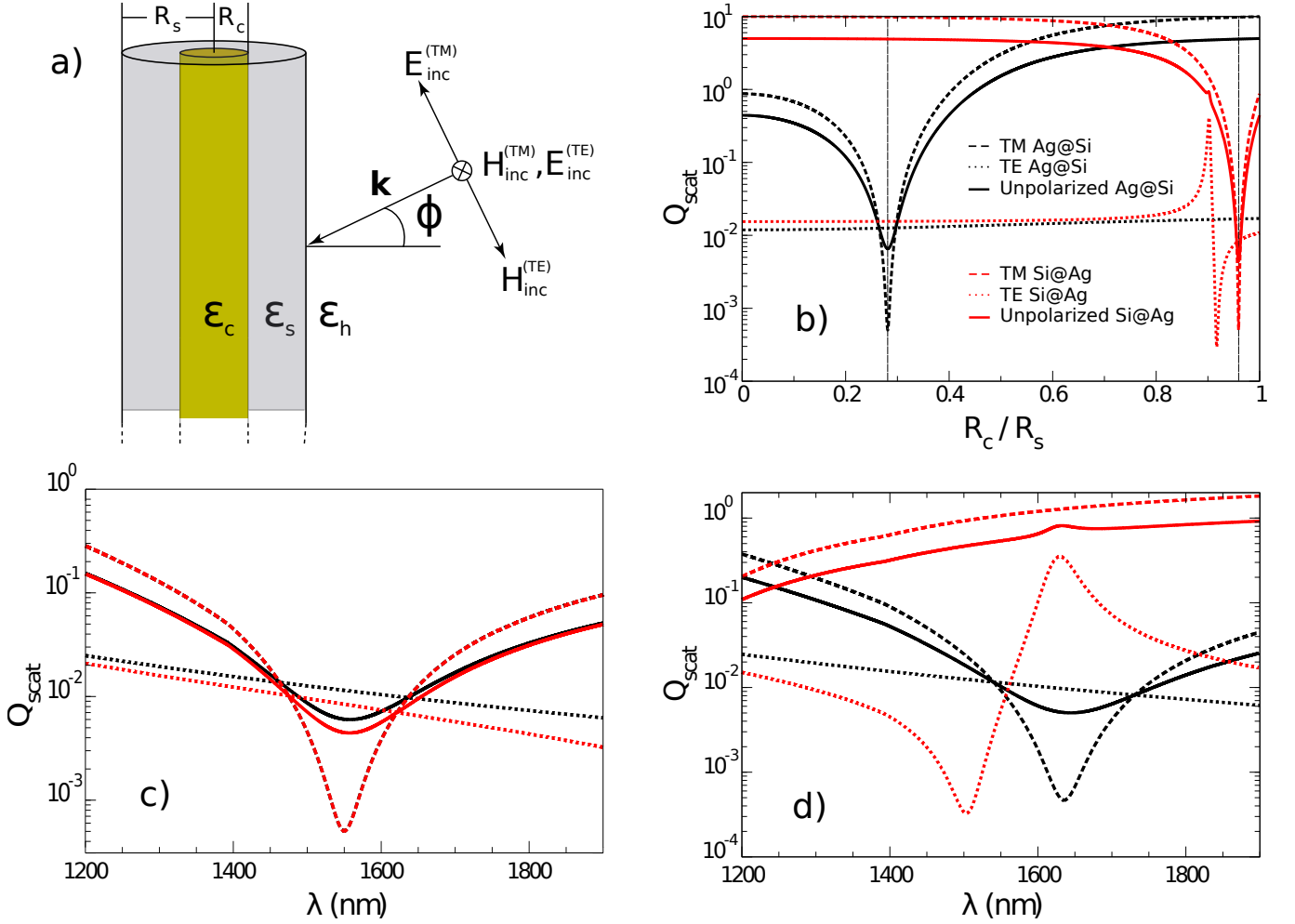


Figure 1. (a) Sketch of the system under consideration together with the relevant parameters. (b-d), scattering efficiency  $Q_{scat}$  as obtained from the quasi-static approximation. TM polarization (dashed line), TE polarization (dotted line) and unpolarized (solid line) radiation is considered for both Ag@Si (black curves) and Si@Ag (red curves) structures. (b)  $Q_{scat}$  at a constant wavelength  $\lambda = 1550$  nm is plotted as a function of the core to shell radii ratio. (c), the spectra for the different polarizations are presented. The size ratio  $R_c/R_s$  is fixed in such a way that  $Q_{scat}$  is minimized in TM polarization for each structure. (d)  $Q_{scat}$  spectra are presented when the core radius is reduced by 5%.

we predict a minimum in the  $Q_{scat}$  at  $R_{tr}^{TE} \simeq 0.917$ . Nevertheless, at a slightly smaller value of the size ratio, as predicted by Eq. (7), a LSP resonance occurs. At  $\lambda = 1550$  nm, the size ratio at plasmon resonance given by Eq. (7) is  $R_{plsp}^{TE} = R_{tr}^{TE} 129/131$ , which is of the order of 1.5% smaller than the optimum size ratio for transparency.

The scattering efficiency spectrum is represented in the region of interest for core-shell dimensions satisfying the optimum condition [see Fig. 1(c)] for TM polarization. As expected, the scattering spectra exhibit a pronounced minimum at the working wavelength of  $\lambda = 1550$  nm for this polarization. In fact, in this case,  $Q_{scat}$  spectra for both Ag@Si and Si@Ag NWs are exactly the same. Moreover, as can be seen in Fig. 1(c), the spectra for Ag@Si and Si@Ag for unpolarized radiation are very similar, with only a small difference due to the TE polarization component.

We might conclude that, Ag@Si NWs behave essentially as Si@Ag if the metal/dielectric volume fraction is kept to the optimum value for achieving transparency at the selected wavelength. Nevertheless, as indicated above, small changes in the size ratio of the structure might lead to large variations in the  $Q_{scat}$  spectrum in TE polarization for dielectric@metal structures. In deed, as can be observed in Fig. 1(d), this is the case when the size ratio is diminished by 5%. The spectrum corresponding to Ag@Si red shifts by about 5.6%, while the spectrum corresponding to Si@Ag varies dramatically, not showing a minimum and increasing its value by a large amount in the whole considered band. This is due to the fact that, at size ratios close to the optimum one, the spectrum of Si@Ag nanowires shows a LSP resonance. In this regard, transparency in metal@dielectric structures is expected to be more robust against structural variations.

From the quasi-static polarizability approximations, we can also obtain useful information regarding the minimum value of the scattering efficiency and bandwidth. We focus on metal@dielectric structures in TM polarization since this structure is, as stated above, more robust against fabrication errors, and the TM polarization controls the scattering spectrum while the TE polarization adds a slowly varying background. The transparency condition given by Eq. (3) links the size ratio of the optimized structure with the real parts of the polarizabilities of the different materials. The chromatic dispersion and the absorption controls the bandwidth of the transparency region and the minimum value of the scattering efficiency respectively.

If we compare the scattering cross-length in TM polarization of the optimized Ag@Si structure with the bare Ag core, we obtain, after some algebra, a scattering cross-length ratio (in this case  $c=\text{Ag}$ ,  $s=\text{Si}$  and  $h=\text{vacuum}$ )

$$\frac{\sigma_s^{(TM, Ag@Si)}}{\sigma_s^{(TM, Ag)}} \simeq \left| 1 + \frac{\epsilon_s - \epsilon_h}{\epsilon_c - \epsilon_h} \frac{\epsilon_c^{(tr)} - \epsilon_h^{(tr)}}{\epsilon_h^{(tr)} - \epsilon_s^{(tr)}} \right|^2 \quad (8)$$

where  $(tr)$  denotes the polarizability value taken at the transparency condition. The optimized structure presents less scattering than the bare one if this ratio is smaller than unity. If we further consider that both host and shell do not show chromatic dispersion, and that the permittivity of the metal is much larger than the host medium one,  $|\epsilon_c| \gg \epsilon_h$ , this ratio simplifies to

$$\frac{\sigma_s^{(TM, Ag@Si)}}{\sigma_s^{(TM, Ag)}} \simeq \left| 1 - \frac{\epsilon_c^{(tr)}}{\epsilon_c} \right|^2 \quad (9)$$

hence, considering relatively small losses in the metal, the core-shell structure scatters less efficiently in a spectral window where  $|\epsilon_c(\lambda)| > 2|\epsilon_c(\lambda_{tr})|$ . In the case of Ag@Si NW in vacuum, this transparency region starts at a wavelength  $\lambda \simeq 1100$  nm for an optimized structure with a scattering minimum at  $\lambda_{tr} = 1550$  nm. At longer wavelengths, the bare silver structure scatters light more efficiently than the core-shell one.

At the minimum scattering wavelength, the scattering efficiency in this configuration can be estimated to be

$$Q_{scat}^{(TM)}(\lambda = \lambda_{tr}) \simeq \frac{\pi^5}{\sqrt{\epsilon_h}} \left( \frac{R_s}{\lambda_{tr}} \right)^3 \left( \frac{\epsilon_c'' \epsilon_h - \epsilon_s'}{\epsilon_c' - \epsilon_c''} \right)^2, \quad (10)$$

where  $\epsilon' = \text{Re}(\epsilon)$  and  $\epsilon'' = \text{Im}(\epsilon)$ . In the example shown in Fig. 1(b), we have  $Q_{scat}^{(TM)}(\lambda = 1550 \text{ nm}) \simeq 5.10 \times 10^{-4}$ , which is of the order of 1% larger than the numerically obtained value.

From Eq. (10) it is clear that the scattering efficiency at the transparency wavelength is determined by the absorption level in the metal (imaginary part of the permittivity) and is smaller the smaller the structure is.

### III. SINGLE AG@SI NW TRANSPARENCY: EXTENDED MIE CALCULATIONS

To check the predictions obtained in the previous section, which were derived by using a quasi-static approximation, we shall focus in this section on Ag@Si cylinders, rigorously calculating scattering cross sections by Mie expansion. We consider a multilayered concentric cylindrical structure; the fields at each layer are suitably expanded as a sum of cylindrical vector harmonics. Solving for the matching conditions at each interface and expanding the incoming plane wave in the same basis, provides an analytic solution of the scattering problem for any incoming radiation direction and polarization [35, 37].

We are interested in the telecommunications range and hence we take a band centered at  $\lambda = 1550$  nm. In Fig. 2(a), a color map of the scattering efficiency ( $Q_{scat}$ ) of a Ag@Si NW is shown. The radius of the shell is kept constant at  $R_s = 45$  nm, while the core radius varies from  $R_c = 0$  nm (pure Si NW) to  $R_c = 45$  nm (pure silver NW). The vacuum wavelength varies in the range  $1000 \text{ nm} \leq \lambda \leq 1900$  nm. For a core radius  $R_s \simeq 14$  nm (white dashed line), the NW presents a scattering efficiency spectrum much weaker than those of either the homogeneous Si or Ag NWs alone [Fig. 2(b)] by one or two orders of magnitude, in the range  $1400 \text{ nm} \leq \lambda \leq 1900$  nm, and for unpolarized radiation. The exact value value of the optimum  $R_s$  for this system is only 7.4% larger than the quasi-static prediction of Eq. (3), which supports the validity of the approximate transparency condition for subwavelength NW dimensions. In fact, for the chosen NW diameter, materials and wavelengths, contributions from higher order multipoles than the ones in the quasi-static approximation are essentially negligible [21]. For the TM polarization, studied in detail in this section, only the monopole mode  $n = 0$  [21, 24] significantly contributes to the scattering cross section, while for the TE mode, only the dipolar mode ( $n = \pm 1$ ) contributes to scattering.

In order to establish a comparison with a simple lossless scattering system, we calculate the scattering efficiency of a thin glass slab (refractive index  $n \simeq 1.45$ ). In this case,  $Q_{scat}$  can be obtained through the Fresnel coefficients of the

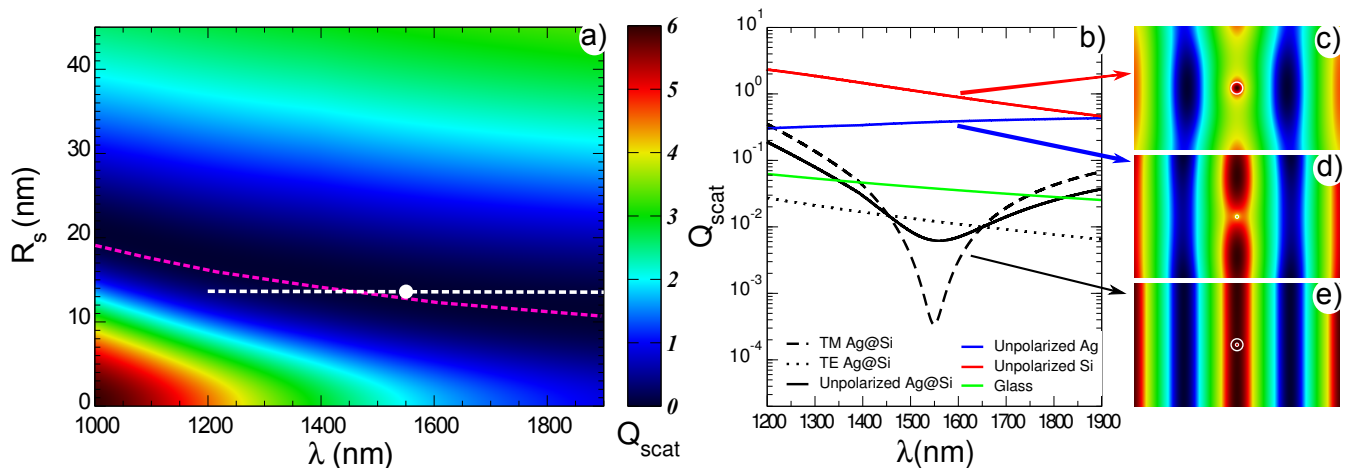


Figure 2. (a) Scattering efficiency spectra as a function of the core (silver) radius for a fixed shell (silicon) outer radius  $R_s = 45$  nm. (b) Scattering efficiency spectra for a Ag@Si core-shell NW ( $R_s = 13.6$  nm,  $R_s = 13.6$  nm) and different polarizations: TM (black dashed), TE (black dotted) and unpolarized (black solid line). For the sake of comparison we also represent  $Q_{scat}$  for a homogeneous Ag NW (red curve,  $R = 13.6$  nm), a homogeneous Si NW (blue curve,  $R = 45$  nm), and for a homogeneous 90 nm thick glass slab (refractive index  $n=1.45$ ). (c-e) Maps of the electric field along the cylinder axis direction in TM polarization at a working wavelength of  $\lambda = 1550$  nm (corresponding to the minimum of the black curve in b). (c) Bare silver NW. (d) Homogeneous silicon NW. (e) Ag@Si NW.

structure. If  $t$  is the transmission coefficient as a function of the wavelength,  $Q_{scat} = 2(1 - \text{Re}(t))$ . Although basic antireflecting coatings might be used to minimize the scattering of the glass slab, it is remarkable that the optimized Ag@Si NW scatters less efficiently than a 90 nm thick glass slab despite the metallic character of the core.

In Figs. 2(c)–2(e), a color map of the electric field along the direction parallel to the cylinder axis is shown for three different cases at  $\lambda = 1550$  nm. The incoming signal is a TM polarized plane wave at normal incidence. The electric field is represented in a plane perpendicular to the cylinder. In Fig. 2(c), a single homogeneous silicon NW is considered (sketched as a circle at the center of the Fig.) of radius  $R = 45$  nm. As can be seen in the Fig., the wave fronts are largely altered due to the interference of the incoming wave with the scattered field. A similar behavior is obtained when a homogeneous silver NW of radius  $R = 13.6$  nm is considered [Fig. 2(d)]. Nevertheless, as shown in Fig. 2(e), when the same silver NW is covered by a 31.4 nm thick silicon shell, the total electric field does not appreciably differ from the plane wave even in the close proximity of the NW surface. Hence the scattering efficiency of the core-shell NW is strongly reduced in this situation.

In order to assess the robustness of transparency regarding the incoming signal, we now consider different incidence angles and polarizations. In Fig. 3(a), an incoming TM polarized plane wave impinges on the core-shell cylinder. In this case we keep the geometry of the system constant ( $R_s = 45$  nm,  $R_s = 13.6$  nm). The scattering efficiency keeps at very low values, of the order of  $10^{-2}$  in a band centered at  $\lambda = 1550$  nm, with band-width is of the order of 200 nm for angles deviating from normal incidence as much as 45 degrees. Hence, we can conclude that the transparency band is very robust against variations in the angle of incidence.

Regarding polarization, it is rather clear that the optimum polarization corresponds to TM. Nevertheless, as shown in Fig. 3(b), low scattering efficiency regions, for normal incidence and linearly polarized light, are quite robust against variations in the polarization state of the incoming light. In this Fig. we show a color map of the scattering efficiency as a function of the angle  $\chi$  between the incoming electric field and the cylinder axis. If  $Q_{\parallel}$  and  $Q_{\perp}$  are the scattering efficiencies for TM and TE polarizations respectively, the scattering efficiency for a general linearly polarized plane wave at normal incidence is  $Q_{scat} = Q_{\parallel} \cos^2(\chi) + Q_{\perp} \sin^2(\chi)$ . Again, a band between  $\lambda = 1400$  nm and  $\lambda = 1850$  nm shows a scattering efficiency  $Q_{scat} \leq 0.05$  for any polarization state.

#### IV. TRANSPARENCY OF NW ASSEMBLIES

We now address the effects due to the multiple scattering of light in arrangements of NWs relatively close to each other. In principle, multiple light scattering can lead to an inhibition or enhancement of radiation scattering depending on the spatial distribution of scatterers, frequency, and parameters describing each cylinder. As shown in Fig. 2(c), the optimum structure barely scatters light and, more importantly, the amplitude of the scattered field in the near

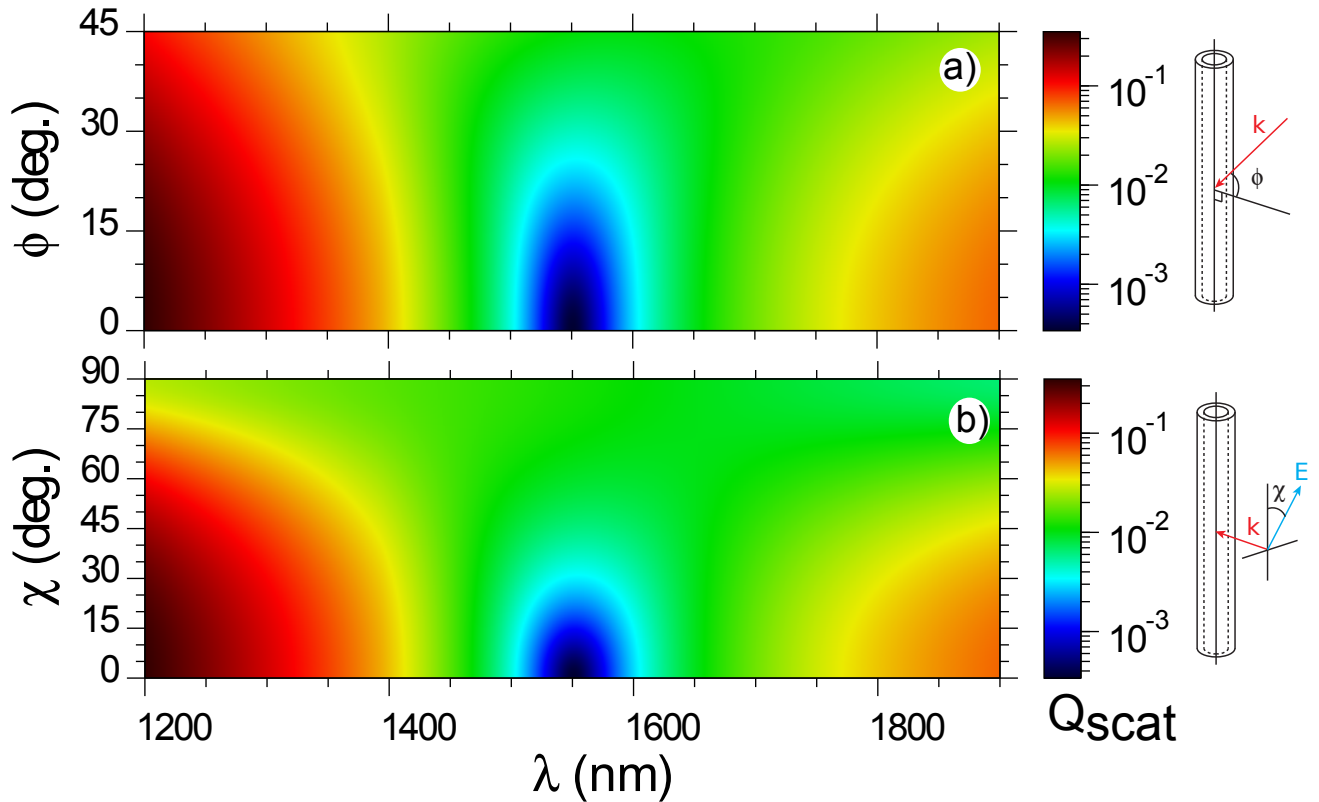


Figure 3. (a) Scattering efficiency spectra for a Ag@Si core-shell NW ( $R_c = 13.6$  nm and  $R_s = 45$  nm) as a function of (a) the angle of incidence ( $\phi$ ) for TE polarized light and (b) the polarization angle ( $\chi$ ) at normal incidence for the same structure.

field region is also much smaller than the amplitude of the incoming plane wave. Hence, we expect to obtain small multiple scattering effects in an assembly of identical randomly distributed NW.

To test this prediction, we numerically calculate scattering efficiencies of NW dimers at different distances and incident radiation conditions and also the scattered fields of assemblies of randomly placed NWs. Numerical simulations were carried out using the RF module of the Finite Element Method based commercial software COMSOL Multiphysics 4.3. Both in the case of the scattering properties of the core-shell NW dimers, as in the simulation of a slab, formed by a random arrangement of these structures, the geometry of the problem is two-dimensional. In the case of dimers, the simulation domain consisted on three concentric circles. While the outer annulus was defined as a Perfectly Matched Layer, in order to absorb all fields and simulate free space propagation, the first boundary was used to perform additional calculations. Core-shell NWs were then defined by two concentric circles placed a distance  $d$  one from each other. Material parameters for air and silicon were taken constant ( $\epsilon_{Si} = 12.25$  and  $\epsilon_{Air} = 1.0$ ), while silver permittivity was taken from [36]. In the case of a slab of randomly arranged NWs, these were distributed in such a way that covered, at least, the whole range of distances and orientations studied in the case of dimers. In this case the simulation domain was a square ( $4.2 \mu\text{m}$  side) and scattering boundary conditions were applied in all exterior boundaries. Scattered field formulation was used in both cases. This built-in option of the program allows one to analytically define the excitation field. This was set to be a plane wave with the electric field pointing out of the simulation plane. Meshing was done with the program built-in algorithm. The mesh consisted on triangular elements, with a maximum element size of 42 nm in the case of the random distribution (20 nm in the case of dimers), a maximum element growth rate of 1.1, meaning that adjacent elements to a given one should not be 1.1 times bigger than it, and a resolution of curvature and narrow regions of 0.2 and 1, respectively. With these parameters, the meshing algorithm automatically increases the mesh quality in narrow and curved regions, such as the core of the wires and the inter-particle spaces. The total number of elements was 176034 in the, computationally more demanding, case of randomly distributed NWs. MUMPS direct solver was used, involving 1258331 degrees of freedom, which, in a desktop machine with 4 processors, required about 3.5 Gb of memory and about 45 seconds per wavelength. In the case of dimers, scattering efficiency was computed integrating the outward normal component of the Poynting vector of the scattered fields in the auxiliary circumference described above, and normalizing by the incident intensity and



geometrical cross section. Results were tested to reproduce Mie exact solution in the case of an isolated nanowire.

We start by calculating the  $Q_{scat}$  of core-shell dimers. In Fig. 4(a) we consider dimers of equal cylinders with the same parameters as in previous Figs. For an incoming TM polarization, and normal incidence,  $Q_{scat}$  spectra are plotted for different surface-to-surface distance between cylinders. The range of distances ( $d$ ) varies from  $d = 0.1 R_s$  to  $d = 10 R_s$  ( $d = 4.5 \text{ nm} - 450 \text{ nm}$ ). As can be seen in Fig. 4(a), the scattering efficiency increases for distances comparable to the cylinder diameter; nevertheless,  $Q_{scat}$  varies only by a factor of two even in the extreme condition of distances much smaller than the cylinder radius.

If the wave vector of the incoming plane wave is still perpendicular to the cylinder axis but contained in the plane defined by the dimer, the variation of the  $Q_{scat}$  with distance between cylinders is also relatively small: As shown in Fig. 4(b),  $Q_{sca}$  increases at much by a factor of two when the cylinders are in close proximity. In this case, a small shift in the position of the minimum of the scattering spectrum is also observed as a function of the distance.

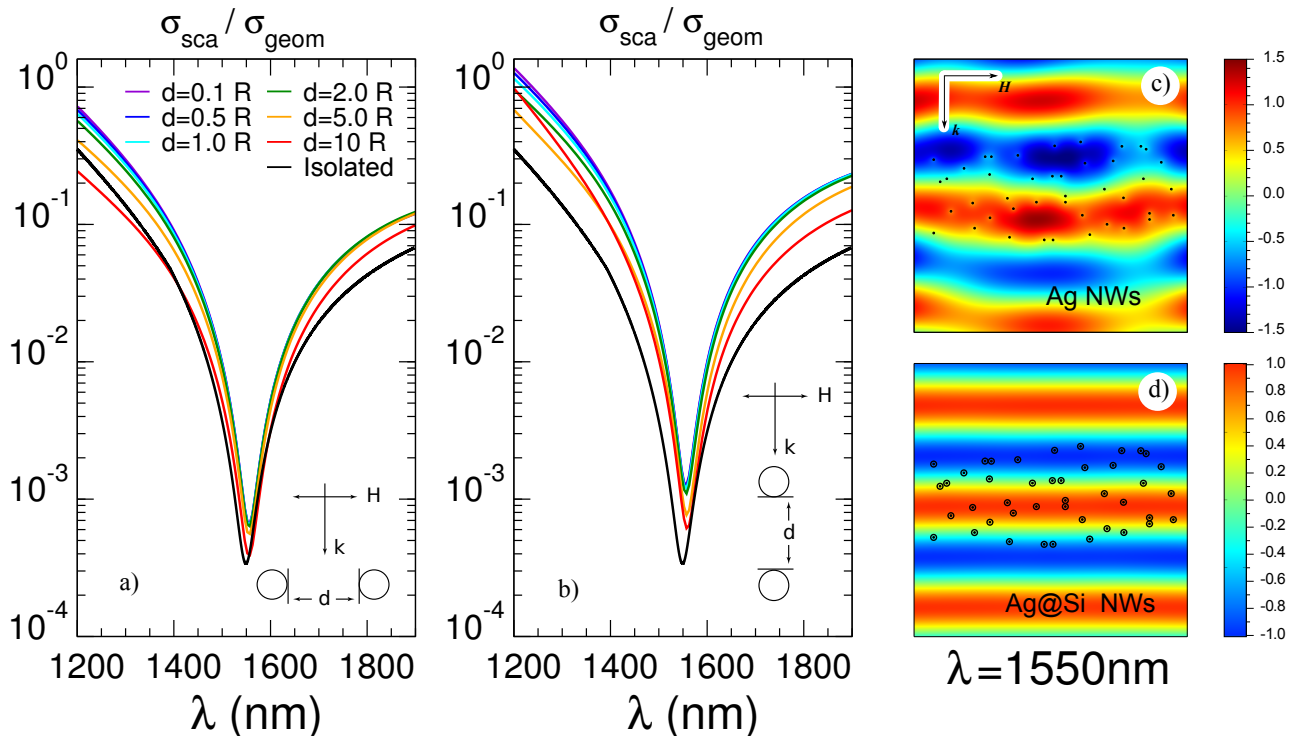


Figure 4. (a) Scattering efficiency of Ag@Si core-shell NW dimers ( $R_s = 13.6 \text{ nm}$ ,  $R_c = 45 \text{ nm}$ ) for TM polarized plane waves with a wave vector perpendicular to the plane defined by the dimer for different distances  $d$  between the nanowires (see legends). (b) Scattering efficiency for the same dimers as in (a), with a wave vector perpendicular to the cylinder axis and in the same plane as the one defined by the dimer. (c) Map of the electric field along the cylinder axis direction at a wavelength of  $\lambda = 1550 \text{ nm}$  for TM polarized waves for an ensemble of bare Ag NWs ( $R = 13.6 \text{ nm}$ ) distributed randomly within a slab. (d) Electric field map corresponding to the the same arrangement of (c). The scattering units in this case are Ag@Si core-shell NWs ( $R_c = 13.6 \text{ nm}$ ,  $R_s = 45 \text{ nm}$ ).

In order to address a more general case, we have compared the scattering by an ensemble of Ag@Si to that of bare Ag cylinders. In Fig. 4(c) we show a color map of the electric field component parallel to the cylinders axes for a random ensemble of bare Ag NWs. The incoming plane wave, at  $\lambda = 1550 \text{ nm}$ , is TM polarized and its propagation direction is perpendicular to the cylinder axes (from top to bottom in the figure). The ensemble of NWs scatters light rather strongly: As can be seen in the figure, the transmitted wave is fully distorted respect to a plane wave. If, for the same positions of the NW axes and identical incoming plane wave, we consider Ag@Si NWs, the scattering is inhibited to a large extent as shown in Fig. 4(d) where, as previously used, the Ag NW is coated with a  $31.4 \text{ nm}$  thick Si layer. The positions of the NWs were generated randomly within a slab of roughly  $4 \mu\text{m}$  by  $1.5 \mu\text{m}$  with the sole restriction of keeping a minimum surface-to-surface distance  $d_{min} \simeq 0.1 R_s$ .

Going one step further, we have increased the density of NW in the arrangement and disordered the structural parameters of each of the cylinders in the structure. In Fig. 5 we show color maps corresponding to the electric field scattered by different ensembles of randomly placed NWs occupying a region of dimensions  $4 \mu\text{m}$  by  $1.5 \mu\text{m}$ . In Fig.



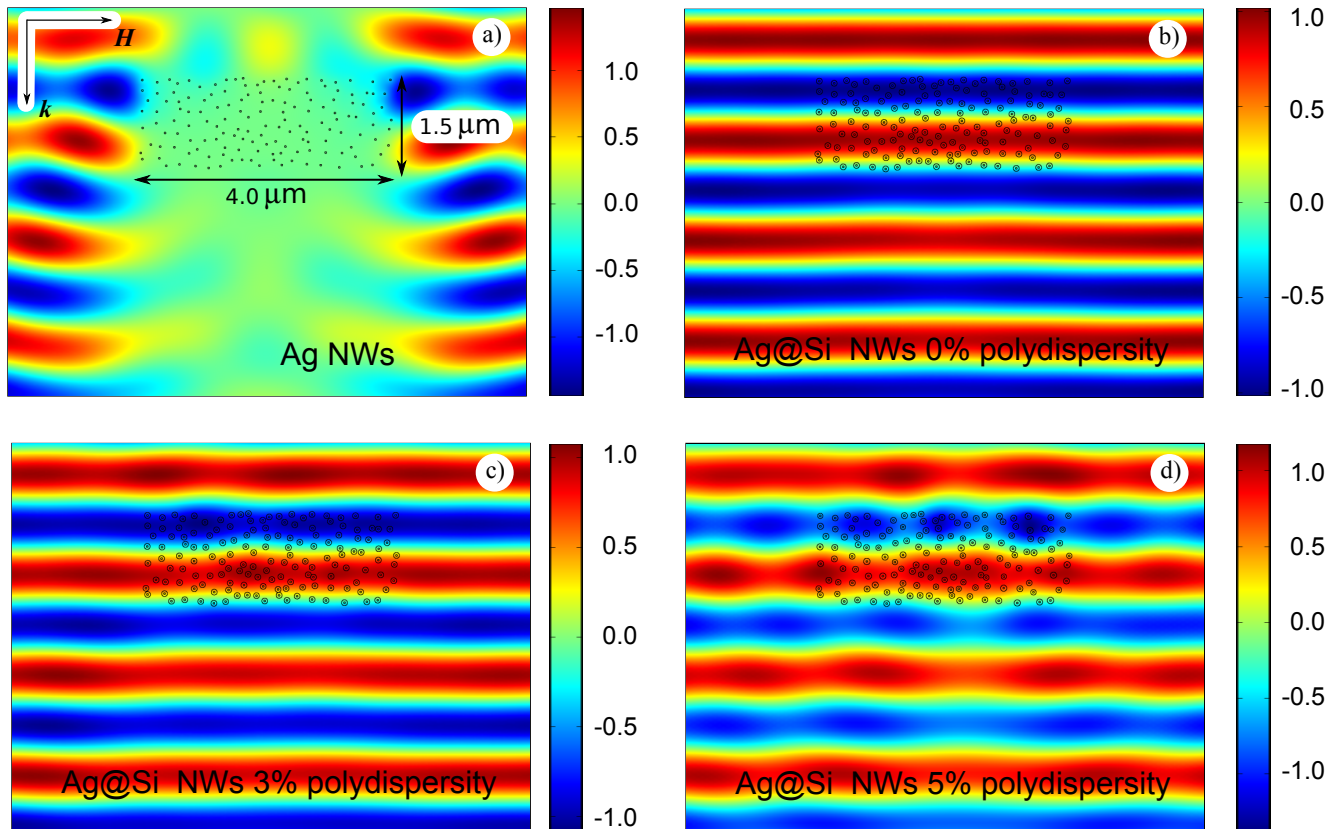


Figure 5. (a) Map of the electric field along the cylinder axis direction at a wavelength of  $\lambda = 1550$  nm for TM polarized waves for an ensemble of bare Ag NWs ( $R = 13.6$  nm) distributed randomly within a slab of  $4\mu\text{m}$  by  $1.5\mu\text{m}$ . (b) Electric field map corresponding to the the same arrangement of (a). The scattering units in this case are Ag@Si core-shell NWs ( $R_c = 13.6$  nm,  $R_s = 45$  nm), the filling fraction of the arrangement is 16%. (c) Electric field map corresponding to the same structure as in (b), with the addition of random disorder in both core and shell radii with a standard deviation of 3% around the optimal values. (d) the same as in (c) with a 5% standard deviation.

5(a), the electric field distribution for bare silver ( $R = 13.6$  nm) NWs is shown. As can be seen, the incoming wave is strongly scattered at the working wavelength ( $\lambda = 1550$  nm).

In Fig. 5(b), the same arrangement, in this case of Ag@Si NWs optimized for transparency, is considered. The filling fraction of the NW ensemble is 16%. Despite this relatively high filling fraction, the electric field map shows that the scattering is very small, definitely much smaller than in the case of bare silver NWs.

In this case, we chose a maximum element size of 4 nm for the silver parts of the system, 10 nm for those of silicon, and 80 nm for the whole air domain. In all cases, we chose the same maximum element growth rate (1.1), resolution of curvature (0.2) and narrow regions (1.0). These settings generate a mesh with 481574 elements in the case in which no polydispersity is assumed. Solution of the system involved 3371719 degrees of freedom, requiring about 6.5 Gb of memory and two minutes per wavelength.

In any realistic application, some fabrication errors are expected. With state-of-the-art techniques, random variations of the core and/or shell radii down to a few percents are achievable. In order to consider this kind of fabrication deviations, we have calculated the light scattering for an assembly of NWs which centers are positioned at the same coordinates as in the cases shown in Fig. 5(a-b) but with some degree of structural disorder. In Fig. 5(c), random variations (normally distributed) of the core and shell radii are introduced with standard deviations of 3% for both parameters. As can be seen in this figure, the wavefronts are slightly disturbed with respect to the optimal case. Even if the structural disorder in the NWs is increased up to a 5% standard deviation, as shown in Fig. 5(d), the transparency condition holds relatively unperturbed.

## V. CONCLUSIONS

We have obtained general conditions under which a core-shell nanowire presents transparency based on the polarizability with radiative corrections of the structures. This approach permits us to obtain relatively accurate, yet simple, analytical expressions for the scattering efficiency spectra of the systems under study, thereby revealing the interplay among materials' optical properties and geometry of the NW. These simple transparency conditions are universal and can be thus extrapolated to any spectral regime provided that the core-shell cylinders are relatively subwavelength.

We have shown that transparency can be achieved with metal@dielectric, dielectric@metal and dielectric@dielectric structures with the appropriate geometrical and optical parameters. Regarding metal-dielectric cylinders, both metal@dielectric and dielectric@metal structures can be designed to be transparent under certain conditions. Nevertheless, we have shown that metal@dielectric structures are much more robust against variations in the geometrical parameters defining the transparent system. By contrast, the appearance of localized surface plasmon resonances for dielectric@metal cylinders close to the transparency condition lead to a large scattering enhancement for slight NW radius variations (namely, imperfections).

By using an exact Mie-based modeling of the core-shell cylinders, we have shown that broad-band transparency of metal@dielectric NWs in the infrared telecommunications range is achievable with realistic materials (i.e. Si-coated Ag nanowires), even higher than glass. Also, this effect is shown to be very robust against relatively large geometrical variations (such as unavoidable fabrication imperfections), and also for a broad range of angles of incidence and polarization.

Moreover, at the transparency condition, scattering is very weak even deep in the near field zone. Indeed, our calculations reveal that an assembly of Ag@Si NWs (even if close to each other) remain highly transparent.

Bear in mind that other metals can also be used: i.e. copper, which exhibits an optical response very similar to that of Ag in this spectral regime. A wealth of semiconductors with high refractive index and low losses could be exploited as well as shells, properly tuning the coating thickness.

This system is hence a suitable building block for electrical wiring where keeping optical transparency is mandatory. Moreover, we anticipate widespread applications of our theoretical analysis on transparency in a variety of hybrid metal-semiconductor nanowires, relevant i.e. to nanophotonics and plasmonics, photovoltaics and metamaterials.

## ACKNOWLEDGMENTS

The authors acknowledge the Spain Ministerio de Economía y Competitividad, through the Consolider-Ingenio project EMET (CSD2008-00066) and NanoLight (CSD2007-00046), and NANOPLAS+ (FIS2012-31070) and FIS2012-3611, and the Comunidad de Madrid (grant MICROSERES P2009/TIC-1476) for support. R. P.-D. and L.S F-P, also acknowledge support from the European Social Fund and CSIC through a JAE-Pre and JAE-Doc grants, respectively.

- 
- [1] P.-Y. Chen, J. Soric, and A. Alù, "Invisibility and cloaking based on scattering cancellation," *Adv. Mater.* **24**, OP281–OP304 (2012).
  - [2] F. Gömöry, M. Solovyov, J. Šouc, C. Navau, J. Prat-Camps, and A. Sánchez, "Experimental realization of a magnetic cloak," *Science* **335**, 1466–1468 (2012).
  - [3] P. Fan, U. K. Chettiar, L. Cao, F. Afshinmanesh, N. Engheta, and M. L. Brongersma, "An invisible metal-semiconductor photodetector," *Nature Photon.* **6**, 380–385 (2012).
  - [4] A. García-Etxarri, R. Gómez-Medina, L. S. Froufe-Pérez, C. López, L. Chantada, F. Scheffold, J. Aizpurua, M. Nieto-Vesperinas, and J. J. Sáenz, "Strong magnetic response of submicron silicon particles in the infrared," *Opt. Express* **19**, 4815–4826 (2011).
  - [5] Q. Zhao, J. Zhou, F. Zhang, and D. Lippens, "Mie resonance-based dielectric metamaterials," *Mater. Today* **12**, 60–69 (2009).
  - [6] J. Geffrin, B. García-Cámara, R. Gómez-Medina, P. Albella, L. Froufe-Pérez, C. Eyraud, A. Litman, R. Vaillon, F. González, M. Nieto-Vesperinas, J. Sáenz, and F. Moreno, "Magnetic and electric coherence in forward- and backscattered electromagnetic waves by a single dielectric subwavelength sphere," *Nat. Commun.* **3**, 1171 (2012).
  - [7] S. Person, M. Jain, Z. Lapin, J. J. Sáenz, G. Wicks, and L. Novotny, "Demonstration of zero optical backscattering from single nanoparticles," *Nano Lett.* **13**, 1806–1809 (2013).
  - [8] Y. H. Fu, A. I. Kuznetsov, A. E. Miroshnichenko, Y. F. Yu, and B. Lukyanchuk, "Directional visible light scattering by silicon nanoparticles," *Nat. Comm.* **4**, 1527 (2013).
  - [9] E. Prodan, C. Radloff, N. J. Halas, and P. Nordlander, "A hybridization model for the plasmon response of complex nanostructures," *Chem. Phys. Lett.* **302**, 419–422 (2003).

- [10] C. S. Levin, C. Hofmann, T. A. Ali, A. T. Kelly, E. Morosan, P. Nordlander, K. H. Whitmire, and N. J. Halas, “Magnetic-plasmonic core-shell nanoparticles,” *ACS Nano* **3**, 1379–1388 (2009).
- [11] R. Paniagua-Domínguez, F. López-Tejeira, R. Marqués, and J. A. Sánchez-Gil, “Metallo-dielectric core-shell nanospheres as building blocks for optical three-dimensional isotropic negative-index metamaterials,” *New J. Phys.* **13**, 123017 (2011).
- [12] W. Liu, A. E. Miroshnichenko, D. N. Neshev, and Y. S. Kivshar, “Broadband unidirectional scattering by magneto-electric core-shell nanoparticles,” *ACS Nano* **6**, 5489–5497 (2012).
- [13] S. Oldenburg, R. Averitt, S. Westcott, and N. Halas, “Nanoengineering of optical resonances,” *Chem. Phys. Lett.* **288**, 243–247 (1998).
- [14] M. Kerker, “Invisible bodies,” *J. Opt. Soc. Am.* **65**, 376–379 (1975).
- [15] H. Chew and M. Kerker, “Abnormally low electromagnetic scattering cross sections,” *J. Opt. Soc. Am.* **5**, 445–449 (1976).
- [16] A. Alù and N. Engheta, “Achieving transparency with plasmonic and metamaterial coatings,” *Phys. Rev. E* **72**, 016623 (2005).
- [17] A. Alù and N. Engheta, “Erratum: Achieving transparency with plasmonic and metamaterial coatings [*Phys. Rev. E*, **72**, 016623 (2005)],” *Phys. Rev. E* **73**, 019906(E) (2006).
- [18] Y. Li, F. Qian, J. Xiang, and C. M. Lieber, “Nanowire electronic and optoelectronic devices,” *Mater. Today* **9**, 18–27 (2006).
- [19] G. Grzela, R. Paniagua-Domínguez, T. Barten, Y. Fontana, J. A. Sánchez-Gil, and J. G. Rivas, “Nanowire antenna emission,” *Nano Lett.* **12**, 5481–5486 (2012).
- [20] A. Tuniz, B. T. Kuhlmeier, P. Y. Chen, and S. C. Fleming, “Weaving the invisible thread: design of an optically invisible metamaterial fibre,” *Opt. Express* **18**, 18095–105 (2010).
- [21] A. Alù, D. Rainwater, and A. Kerkhoff, “Plasmonic cloaking of cylinders: finite length, oblique illumination and cross-polarization coupling,” *New J. Phys.* **12**, 103028 (2010).
- [22] P. Mundru, V. Pappakrishnan, and D. Genov, “Material- and geometry-independent multishell cloaking device,” *Phys. Rev. B* **85**, 045402 (2012).
- [23] Y. Huang, Y. Feng, and T. Jiang, “Electromagnetic cloaking by layered structure of homogeneous isotropic materials,” *Opt. Express* **15**, 11133–11141 (2007).
- [24] A. Mirzaei, I. V. Shadrivov, A. E. Miroshnichenko, and Y. S. Kivshar, “Cloaking and enhanced scattering of core-shell plasmonic nanowires,” *Opt. Express* **21**, 10454–10459 (2013).
- [25] Y. Urzhumov, N. Landy, T. Driscoll, D. Basov, and D. R. Smith, “Thin low-loss dielectric coatings for free-space cloaking,” *Opt. Lett.* **38**, 1606–1608 (2013).
- [26] R. Paniagua-Domínguez, D. R. Abujetas, and J. A. Sánchez-Gil, “Ultra low-loss, isotropic optical negative-index metamaterial based on hybrid metal-semiconductor nanowires,” *Sci. Rep.* **3**, 1507 (2013).
- [27] S. Lal, J. H. Hafner, N. J. Halas, S. Link, and P. Nordlander, “Noble metal nanowires: from plasmon waveguides to passive and active devices,” *Acc. Chem. Res.* **45**, 1887–1895 (2012).
- [28] A. Kim, Y. Won, K. Woo, C.-H. Kim, and J. Moon, “Highly transparent low resistance ZnO/Ag nanowire/ZnO composite electrode for thin film solar cells,” *ACS Nano* **7**, 1081–1091 (2013).
- [29] K. Ellmer, “Past achievements and future challenges in the development of optically transparent electrodes,” *Nature Photon.* **6**, 809–817 (2012).
- [30] S.-K. Kim, R. W. Day, J. F. Cahoon, T. J. Kempa, K.-D. Song, H.-G. Park, and C. M. Lieber, “Tuning light absorption in core/shell silicon nanowire photovoltaic devices through morphological design,” *Nano Lett.* **12**, 4971–4976 (2012).
- [31] A. Alù and N. Engheta, “Cloaking a sensor,” *Phys. Rev. Lett.* **102**, 233901 (2009).
- [32] R. Paschotta, *Encyclopedia of laser physics and technology* (Wiley, 2008).
- [33] S. Albaladejo, R. Gómez-Medina, L. S. Froufe-Pérez, H. Marinchio, R. Carminati, J. F. Torrado, G. Armelles, A. García-Martín, and J. J. Sáenz, “Radiative corrections to the polarizability tensor of an electrically small anisotropic dielectric particle,” *Opt. Express* **18**, 3556–67 (2010).
- [34] C. F. Bohren and D. R. Huffman, *Absorption and scattering of light by small particles* (John Wiley & Sons, 1998).
- [35] G. A. Shah, “Scattering of plane electromagnetic waves by infinite concentric circular cylinders at oblique incidence,” *Mon. Not. R. Astron. Soc.* **148**, 93–102 (1970).
- [36] P. B. Johnson and R. W. Christy, “Optical constants of the noble metals,” *Phys. Rev. B* **6**, 4370–4379 (1972).
- [37] M. Kerker and E. Matijevic, “Scattering of electromagnetic waves from concentric infinite cylinders,” *J. Opt. Soc. Am.* **51**, 506–508 (1961).